

Light and fluorescence microscopy

Tissue sections stained with hematoxylin/eosin or toluidine blue were mounted with Permount (SP15-500, Fisher Scientific, Pittsburgh, PA) and cover slipped. Microscopy images were obtained with a DP70 color Bayer mosaic digital camera, Peltier device cooled to -10°C , (Olympus America). Tissue sections for fluorescence microscopy images were mounted with SlowFade Gold antifade reagent with 4,6-diamidino-2-phenylindole (DAPI) (Invitrogen, Molecular Probes, Eugene, OR) and cover slipped, and images were obtained with a Soft Imaging Solutions FVII cooled monochrome digital camera, Peltier cooled to -10°C (Olympus America). Ear whole mount pseudo-stacks were collected using Extended Focal Imaging (EFI) (MicroSuite Version 5, Olympus Soft Imaging Solutions, Lakewood, CO) on an Olympus BX61 microscope equipped with a fully automated stage). EFI uses contrast algorithms to create a single in-focus image from a series of images taken at different Z-depth for thick tissue sections. Objectives used were UPlanApo $10\times/0.40$ and $20\times/0.70$.

Confocal microscopy

All confocal Z-stack images were obtained using an Olympus FV1000 confocal microscope running FluoView version 1.7a software (Olympus). A Multi-Argon laser (488/543) at 5% power and a Helium-neon laser (543/618) at 15% were used to sequentially capture images of Alexa Fluor 488 and Alexa Fluor 594-labeled targets, respectively. Using an UPlanApo $100\times/1.35$ numerical aperture Oil-Immersion objective (Olympus), slices were taken at every $0.47\ \mu\text{M}$ through the specimen. Images of individual slices were reassembled and compressed into one final image using the Z-stack feature of ImageJ 1.42q.¹

Immunostaining

Five-micron 10% buffered formalin-fixed tissue sections (HIF-1 α transgene immunostaining), and ethanol-fixed tissue sections ($5\ \mu\text{m}$)(VEGF and keratin-14 dual immunofluorescence, and endothelial and pericyte markers) were deparaffinized, washed in PBS, and blocked (Protein Block, X0909; Dako, Carpinteria, CA) for 30 min at room temperature. The following antibodies, dilutions, and signal enhancements were used: rabbit anti-mouse HIF-1 α [1:10,000; EP1215Y; Epitomics, Burlingame, CA. (HIF-1 α signal was enhanced using tyramide signal amplification kit (T20922; Invitrogen)], chicken anti-mouse VEGF (1:100; ab14078; Abcam, Cambridge, MA), rabbit anti-mouse K14 (1:10,000; PRB-155P; Covance, Princeton, NJ), rat anti-mouse MECA32 (1:50; 550563; BD Bioscience, San Jose, CA), rabbit anti-human vWF (1:10,000; A0082; Dako), rabbit anti-mouse VEGFR2 (1:1000; 2479; Cell Signaling), rabbit anti-mouse SDF-1 (1:1000; 14-7992; eBioscience, San Diego, CA), rabbit anti-mouse desmin (1:300; ab8592; Abcam), rabbit anti-mouse PDGFR β (1:3000; ab32570; Abcam), rabbit anti-mouse NG2 (1:600; AB5320; Millipore), and rabbit anti-mouse αSMA (1:500; ab32575; Abcam), rabbit anti-mouse Cyclin D1 (1:1000; 2978; Cell Signaling), rabbit anti-mouse p21 (1:1000; sc-397; Santa Cruz) and rabbit anti-mouse γH2AX (1:1000; 9718; Cell Signaling). Dual immunofluorescence for endothelial and myeloid cell markers was performed on 4% paraformaldehyde-fixed $10\ \mu\text{m}$ cryosections with the following antibodies: rat anti-mouse CD31 (1:1000; 550274; BD Bioscience), Armenian hamster anti-mouse CD31 (1:2000; MAB1398Z; Millipore, Billerica, MA), rat anti-mouse: CD45 (1:300; 550539; BD Bioscience), CD11b (1:2000; 550282; BD Pharmingen), F4/80 (1:1000; MCA771GA; Serotec, Raleigh, NC) and clone 7/4 (1:1000; CL8993AP; Cedarlane Laboratories; Hornby, Ontario); and rabbit anti-mouse SDF1 α (1:1000; 14-7992; eBioscience; San Diego, CA). All primary antibodies incubations were

done overnight at 4°C. Endothelial cells were identified with DyLight 549-labelled Goat anti-Armenian hamster IgG (1:1000; 127-505-160; Jackson ImmunoResearch; West Grove, PA) or Alexa Fluor 594-labelled goat anti-rat (1:400; A11007; Molecular probes), pericytes with Alexa Fluor 488-labelled goat anti-rabbit (1:400; A11034; Molecular probes); and myeloid cells with Alexa Fluor 488-labelled goat anti-rat (1:400; A11006; Molecular probes) for 1hr at room temperature. Nuclei were counterstained using Slow Fade Gold with 4', 6-diaminoindole (DAPI) (S36938; Invitrogen) or To-Pro-3 (642/661) (1:800; T3605; Invitrogen) applied with secondary antibody (Fig. S5B).

Determination of endothelial cell proliferation

Five-micron sections were treated in 2N HCL for 40 min, washed in deionized water/PBS and incubated at room temperature with 0.01 % protease for 1 min. Sections were PBS washed, blocked and incubated with anti-mouse FITC-BrdU (1:20; MD5420; Invitrogen) and MECA32 (1:20) antibodies overnight at 4°C. Following PBS washing, sections were incubated with Alexa Fluor 594-conjugated goat anti-rat secondary antibody (1:400, Molecular Probes) for 1 hour at room temperature, followed by mounting with Slow Fade Gold.

Quantification of microvessel density, pericyte coverage, proliferating and apoptotic endothelial cells

To evaluate vascular density, the number of MECA32 positive blood vessels in 4–6 10× fields per section/mouse (n=4–8 mice), were counted twice using image analysis software (MicroSuite Version 5). Percentage of proliferating or apoptotic endothelial cells was determined by dividing the mean number of BrdU- or activated caspase3-positive endothelial cells per 4–6 10× fields, by the mean number of MECA32 positive vessels in the same counting area.

Total RNA isolation and real-time RT-PCR analysis

Ears were homogenized in 1 ml TRIzol (15596-018; Invitrogen), total RNA extracted according to the manufacturer's protocol, and reverse transcribed using Superscript II reverse transcriptase (Invitrogen). Real time RT-PCR analysis was performed with primers and TaqMan probes specific for HIF-1 α , VEGF, PlGF, PDGF-B, ADM, SDF-1 α , Glut1, PDK, CAIX, iNOS, TSP-1 and -2 or Histone 3.3A (Table S1). Primer express software was used to design primer/probe sets (Table S1) for gene amplification. Target cDNAs were normalized to histone 3.3A.²

Western blotting

Total protein (120 μ g) was separated on sodium dodecyl sulphate/4–12% polyacrylamide Tris-Glycine gradient Midi gels (WT4121BX10; Invitrogen) and transferred to PVDF membranes (iBlot Gel Transfer Stacks PVDF Regular; IB4010-01; Invitrogen). Membranes were blocked for 1hr at room temperature with gentle shaking in TBST (50 mM Tris, pH 7.6, 150 mM NaCl, 0.1% Tween 20) containing 5% BSA. Membranes were first probed with rabbit monoclonal anti-mouse phospho-VEGFR2^{Y1175} (2478; Cell Signaling) or rabbit anti-mouse phospho-ERK1/2^{T202/Y204} (4376; Cell Signaling) or rabbit polyclonal anti-mouse phospho-PLC γ ^{Y783} (2821; Cell Signaling) or rabbit monoclonal anti-mouse phospho-AKT^{S473} (4058; Cell Signaling) or rabbit anti-mouse phospho-p53^{S20} (9287; Cell Signaling) or γ H2AX^{S139} (9718; Cell Signaling) at 1:1000 dilution, stripped in multiple washes of boiled 100 mM glycine and wash buffer (TBST) (iBlot stripping protocol; Invitrogen) at room temperature and sequentially re probed with rabbit monoclonal anti-mouse VEGFR2 (2479; Cell Signaling); goat anti-mouse VE-

Cadherin (sc-6458; Santa Cruz, Santa Cruz, CA); rabbit polyclonal anti-mouse ERK1/2 (9102; Cell Signaling); rabbit polyclonal anti-mouse PLC γ (2822; Cell Signaling); rabbit polyclonal anti-mouse AKT (9272; Cell Signaling); rabbit anti-mouse p53 (NCL-p53-CM5p; Leica Microsystems, Newcastle upon Tyne, UK); rabbit anti-mouse p21 (sc-397; Santa Cruz); rabbit anti-mouse Cyclin D1 (2978; Cell Signaling) at 1:1000 dilution. After overnight incubation at 4°C, membranes were incubated for 1hr at room temperature in horseradish peroxidase-linked anti-rabbit (1:2000; sc-2301, Santa Cruz) or anti-goat IgG antibodies (1:2000; sc-2304; Santa Cruz) in TBST with 5% non-fat milk and developed in ECL plus reagent (RPN2132; GE Healthcare, Piscataway, NJ). Protein bands were quantified by densitometry, and protein loading normalized to rabbit polyclonal antibody against β -tubulin (1:35,000; ab6046; Abcam, Cambridge, MA).

VEGF, PIGF and SDF-1 α ELISA

Liquid nitrogen snap-frozen ear tissues were homogenized in 1 \times PBS, 1% NP-40, 1% Sodium deoxycholate, 0.1% SDS, 1 mM EDTA and fresh protease inhibitor cocktail (P8340; Sigma), the homogenate incubated on ice for 30 min, centrifuged for 15 min at 14,000 rpm, and the protein concentration determined (BCA assay kit; 23227; Pierce). The results were normalized to amount of total protein, 20 μ g (VEGF) or 30 μ g (PLGF) or 100 μ g (SDF-1 α). To determine plasma VEGF, PIGF and SDF-1 α , ~900 μ l of peripheral blood was collected by intracardiac puncture under terminal Avertin anesthesia into EDTA coated 2 ml tubes (BD367841; VWR; Batavia, IL), centrifuged at 2000 \times g within 15 min of collection at 4°C for 20 min to isolate plasma and stored at -80°C. VEGF, PIGF and SDF1 ELISA's were performed on undiluted plasma following manufacturer's instructions (R&D Systems).

Immunoblocking antibodies

For VEGFR2 or VEGFR1 immunoblockade, 800 μ g of DC101, MF1 (generous gifts from ImClone Systems, NY, NY), or nonspecific rat IgG (012-000-003; Jackson) were administered i.p. three times per week starting on d0 or d14 of DOX induction of TetON-HIF-1 or DOX treated NTG controls. Following treatment, mice were either anesthetized for noninvasive live L-PAM imaging, or lectin perfused, sacrificed by intracardiac paraformaldehyde perfusion, and ears collected for cross-sectional or whole mount analysis.

Bone marrow cell isolation and transplantation

Recipient age-matched DTG and NTG mice were irradiated with a single dose of 1000 cGy and maintained on antibiotics (trimethoprim-sulfamethoxazole; Alparma, Baltimore, MD) in the drinking water for two weeks post transplantation. Bone marrow (BM) cells were harvested from 6–10 wk old CMV-actin-EGFP transgenic mice, congenic in the FVB/n background (Jackson Labs). Briefly, tibias and femurs were obtained from anesthetized mice and placed on ice in a 6-welled plastic dish. Tibia and femur from one mouse were aseptically flushed with 3 ml sterile PBS. Unfractionated EGFP-BM cells (2×10^6 cells) were injected into TetON-HIF-1 and NTG retro-orbitally 24hr post-irradiation. Chimerism was assessed in recipient mice 6 weeks post-transplantation, using peripheral blood flow cytometry, and determination of the frequency of EGFP cells among peripheral nucleated blood cells after hemolysis by ammonium chloride to eliminate erythrocytes. Mice with 97% chimerism were used in the experiments.

***In vivo* noninvasive label-free longitudinal photoacoustic microscopy (L-PAM)**

A schematic of the L-PAM system is presented in (Fig. S2A). In photoacoustic imaging, the target tissue is usually irradiated by a short-pulsed (~ns) laser beam. Wideband ultrasonic waves (referred to as photoacoustic waves) are induced as a result of transient thermoelastic expansion due to the tissue's absorption of optical energy. As a predominant endogenous light absorber, hemoglobin enables photoacoustic imaging of the microcirculation without angiographic contrast agents.⁴⁻⁶ Thus, blood vessels to be detected by label-free photoacoustic imaging must contain RBCs, the carriers of hemoglobin. This unique characteristic allows L-PAM to selectively image RBC-perfused capillaries, the functional capillary subset supplying oxygen to living tissues; however, exogenous contrast agents such as Evans blue can be used to image all perfused vessels as well.⁷ In the present study, an isosbestic point of the hemoglobin absorption spectrum (570 nm) was chosen. Thus, the detected photoacoustic signal reflects the volumetric distribution of the total hemoglobin concentration, regardless of the blood oxygen level. Our L-PAM system employs diffraction-limited optical focusing with bright field illumination to achieve micrometer lateral resolution (Fig. S2A). The photoacoustic excitation source is a wavelength-tunable dye laser (CBR-D, Sirah, Kaarst, Germany) pumped by a Nd:YLF diode-pumped solid-state laser (INNOSLAB, Edgewave, Wuerselen, Germany). The pulsed laser beam (7-ns pulse width; ≤ 5 kHz pulse repetition rate, tunable) from the dye laser is attenuated before passing through a 25- μm pinhole (P25C; Thorlabs, Newton, NJ) and then is focused by a microscopic objective (RMS4X, Thorlabs). An optical beam splitter is inserted between the pinhole and the objective to aid in-system alignment and image localization through an eyepiece. A homemade acoustic-optical beam splitter, consisting of two right-angle prisms (NT32-545; Edmund Optics, Barrington, NJ) and a 100- μm thick layer of silicone oil (1000cSt, Clearco Products, Bensalem, PA), is located under the microscope objective to separate optical illumination and acoustic detection. A 75 MHz ultrasonic transducer [V2022 (BC); Olympus NDT, Kennewick, WA] is attached to the vertical side of the bottom prism. An acoustic lens (0.46 NA; 5.2 mm radius of curvature) is attached to the bottom of the splitter and immersed in the water tank to collect photoacoustic signals. An open imaging window in the bottom of the water tank is sealed with an ultrasonically and optically transparent polyethylene membrane. Ultrasonic gel (Clear Image; SonoTech, Bellingham, WA) is applied between the polyethylene membrane and the animal tissue for acoustic coupling. The photoacoustic signal detected by the ultrasonic transducer is amplified by two cascaded amplifiers (ZFL 500LN; Mini-Circuits, Brooklyn, NY) and then is digitized by a 14-bit data acquisition (DAQ) board (CompuScope 14200; Gage Applied Sciences, Lockport, IL) at a sampling rate of 200 MS/s. Along the transverse (x - y) plane, 2-D raster scanning of the water tank and the animal together is controlled by a separate PC, which triggers both the DAQ board and the pump laser. The trigger signal is synchronized with the clock-out signal from the DAQ board. The 2-D transverse scanning, in combination with the depth-resolved ultrasonic detection, provides complete 3-D microvascular information, which can be viewed in a direct volumetric rendering or a maximum amplitude projection image. A transmission-mode optical microscope is integrated into our system by adding a light-emitting diode beneath the animal holder. Utilizing the reverse optical path of the L-PAM illumination, the imaging region can be viewed under the eyepiece. This addition helps us to quickly target the same region of the animal, which plays an important role in longitudinal studies of the same animal.

L-PAM for microvessel classification, extraction, and quantitative analysis of vascular subsets

Before quantitative analysis, the photoacoustic signal amplitude in each image was extracted through a Hilbert transformation of the recorded data, and image registration and vessel segmentation were performed using a MATLAB Image Processing Toolbox (R2008a, MathWorks, Boston, MA). The first step is to co-register the volumetric images acquired at different time points to the d0 control image using a 3-D rigid registration (linear translation and/or rotation). Typically 10–20 pairs of points were manually selected from the d0 image and the image to be registered based on the similarity in vascular morphology. Then a spatial translation and rotation matrix was computed for image registration based on the coordinates of these point pairs. The second step is to identify and isolate each single vessel from the vasculature network using vessel segmentation. Each vessel was identified and labeled by tracking its axis in 3-D space. The daughter vessels branching from the mother vessel were labeled as different vessels. The third step is to categorize individual vessels into either the arteriovenous vasculature or capillaries, primarily based on the vessel diameter. Capillaries have an average diameter of 5–10 μm , which is smaller than the arteriovenous vasculature. Thus, 10 μm was set to be the threshold diameter. Besides, depth information and signal intensity were also extracted to help discriminate capillary beds from the arteriovenous vasculature. Finally, the volumes of the capillaries, the arteriovenous vasculature, and the total microvasculature were calculated by integrating the corresponding image voxels, respectively. For multi-day monitoring, the vessel volumes at different time points were normalized to the volumes calculated in d0.

Based on vessel segmentation, the vessel length and tortuosity were further quantified by tracing the vessel axis. First, the center of each vessel cross section was identified. Then, the vessel axis was obtained by connecting all the centers. The vessel length between two adjacent bifurcation points of the selected vessel trunk was measured along the vessel axis (Fig. S2D,F–G). Vessel tortuosity is defined as the ratio of the vessel length to the linear distance between the two bifurcation points (Fig. S2D, green curve). The same artery-vein pair was chosen for the tortuosity quantification at each time point of the 60-day monitoring. The vessel lengths at different time points were normalized to the length in d0.

Table S1. Real-time primer-probe sets used for RT-PCR HIF-1 target gene expression analysis

Real time PCR primers/TaqMan probes (5'–3')

Human HIF-1 α

Forward AAGCAGTAGGAATTGGAACATTATTACA
Reverse AGATTTGCATCCTTTTACACGTTTC
Primer probe AGCCAGACGATCATGCAGCTACTACATCACTT

Mouse Glut1

Forward GCCCAGGTGTTTGGCTTAGA
Reverse TGGGACGAAGACGACACTGA
Primer probe CACAAGTCTGCATTGCCCATGATGG

Mouse CAIX

Forward GATTCTCGGCTACAACACTGA
Reverse GGGAAGGAAGCCTCAATCGT
Primer probe TCCGAGCCACGCAACCCTTGA

Mouse VEGF

Forward GCAGGCTGCTGTAACGATGA
Reverse GTGAGGTTTGATCCGCATGA
Primer probe CCCTGGAGTGCGTGCCCA

Mouse PIGF

Forward TGGTGCCTTTCAACGAAGTG
Reverse CATCCAAGATGTACACCAGCTTCT
Primer probe TCGCAGCTACTGTCGGCCCATG

Mouse SDF-1 α

Forward GAGCCAACGTCAAGCATCTG
Reverse CAGCCGTGCAACAATCTGAA
Primer probe AAATCCTCAACACTCCAAACTGTGCC

Mouse ADM

Forward AAGCCCACATTCGTGTCAAAC
Reverse GAAGCGGCATCCATTGCT
Primer probe CTACCGCCAGAGCATGAACCAGGGT

Mouse iNOS

Forward TGACGGCAAACATGACTTCAG
Reverse GCCATCGGGCATCTGGTA
Primer probe TTCACAGCTCATCCGGTACGCTGG

Mouse PDGF-B

Forward ATAACCGCAATGTGCAATGC
Reverse TCGCACAATCTCAATCTTTCTCA
Primer probe CCGGCCGCATCTGCACCTG

Mouse Ang-2

Forward CTGTGCGGAAATCTTCAAGTCA
Reverse CCTTGATCTCCTCTGTGGAGTTG
Primer probe CACCAGTGGCATCTACACACTGACCTTCC

Mouse TSP-1

Forward CTTCTTCATCAACACCGAGAGAGA
Reverse AGTAGGACTGGGTGACTTGTTTCC
Primer probe CTACCAGTCCAGCAGCCGCTTCTACGTT

Mouse Histone 3.3A

Forward CGTGAAATCAGACGCTATCAGAA
Reverse TCGCACCAGACGCTGAAAG
Primer probe TCCACTGAACTTCTGATCCGCAA

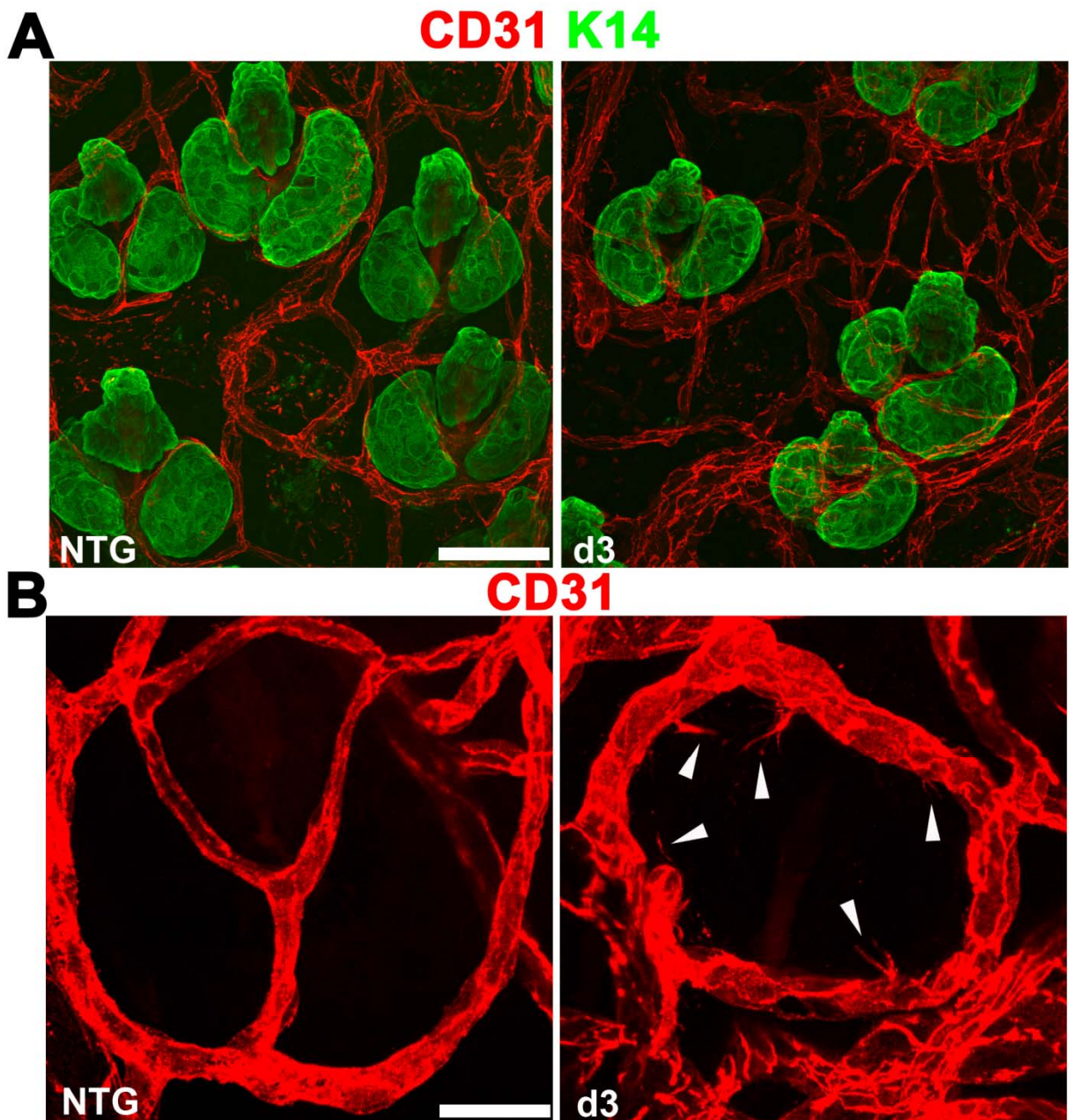
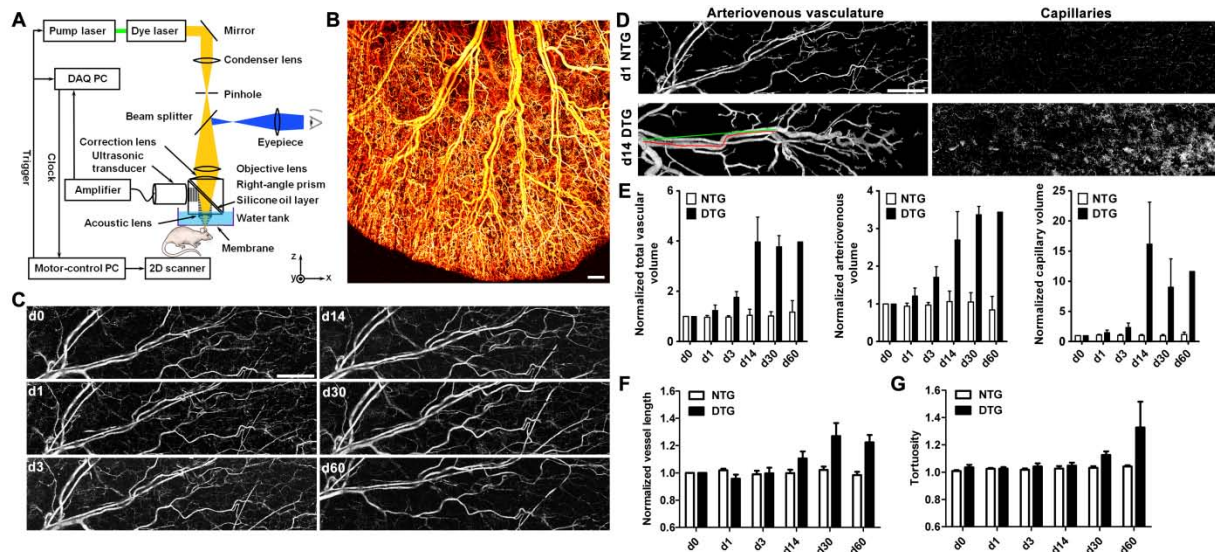


Figure S1. Relationship of transgene expressing epithelial cells and neocapillary genesis in TetON-HIF-1 mice

(A) Representative ear whole mounts demonstrating decoration of the K14/K5 (here K14) follicle outer root sheath keratinocytes and sebaceous glands (green) by CD31 (+) microvessel endothelial cells (red). Keratins -14 and -5 are coordinately expressed, and in TetON-HIF-1 mice, the green cells express the HIF-1 α transgene. (B) Representative whole mounts showing TetON-HIF-1 endothelial tip cells (CD31 immunofluorescence) extending filopodia towards transgene expressing basal and sebaceous gland cells. Bars: (A) 50 μ m; (B) 20 μ m.



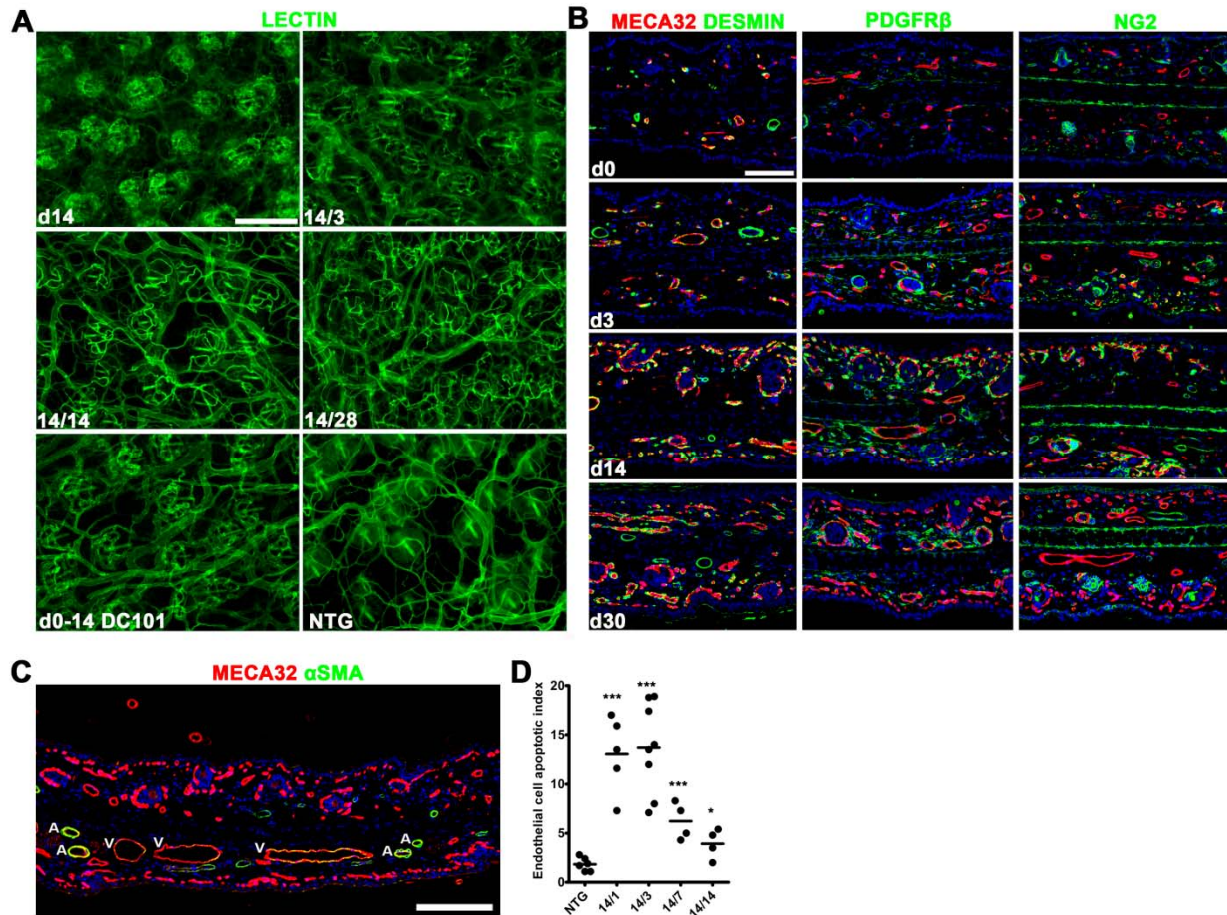


Figure S3. Epithelial HIF-1 activation produces both transgene dependent and independent vessel subtypes, and dynamic alterations of pericyte marker expression over time

(A) FITC-*Lycopersicon esculentum* perfused ear whole mounts demonstrate perifollicular neocapillary development between d0-14, microvessel dropout evident by withdrawal day 3 (14/3), and persistence of the neovasculature that developed at a distance from the hair follicle units after 14 (14/14) or 28 (14/28) days of DOX withdrawal. DOX 0–14 VEGFR2 blockade (DC101) produces a similar microvascular pattern as 14 or 28d withdrawal with extensive dropout of perifollicular capillary clusters. (B) Representative dual MECA32/Desmin (left column) or PDGFR β (middle column) or NG2 (right column) immunofluorescent images. Desmin expression is persistent throughout the course of neovascular development and maintenance in TetON-HIF-1 mice. In contrast, HIF-1 activated pericytes incrementally express PDGFR β and NG2 during the DOX d0–14 development stage, followed by downregulation of these markers during the DOX d14–30 maintenance stage. (C) Representative TetON:HIF-1 DOX d60 mouse showing vessel categorization into vein (V), artery (A) and capillaries (rest of the vessels $\leq 10 \mu\text{m}$) based on their morphology (wall thickness and shape) and smooth muscle actin (αSMA) staining. (D) Quantification of apoptotic indices over time (see Figure 3C for representative dual MECA32/Caspase-3 immunofluorescence). TetON-HIF-1 data at each DOX day were compared with NTG or TetON-HIF-1 d0 data (data not shown), using unpaired Student's t-test (* $P < 0.05$ and *** $P < 0.001$). Bars: (A), 100 μm ; (B, C), 200 μm .

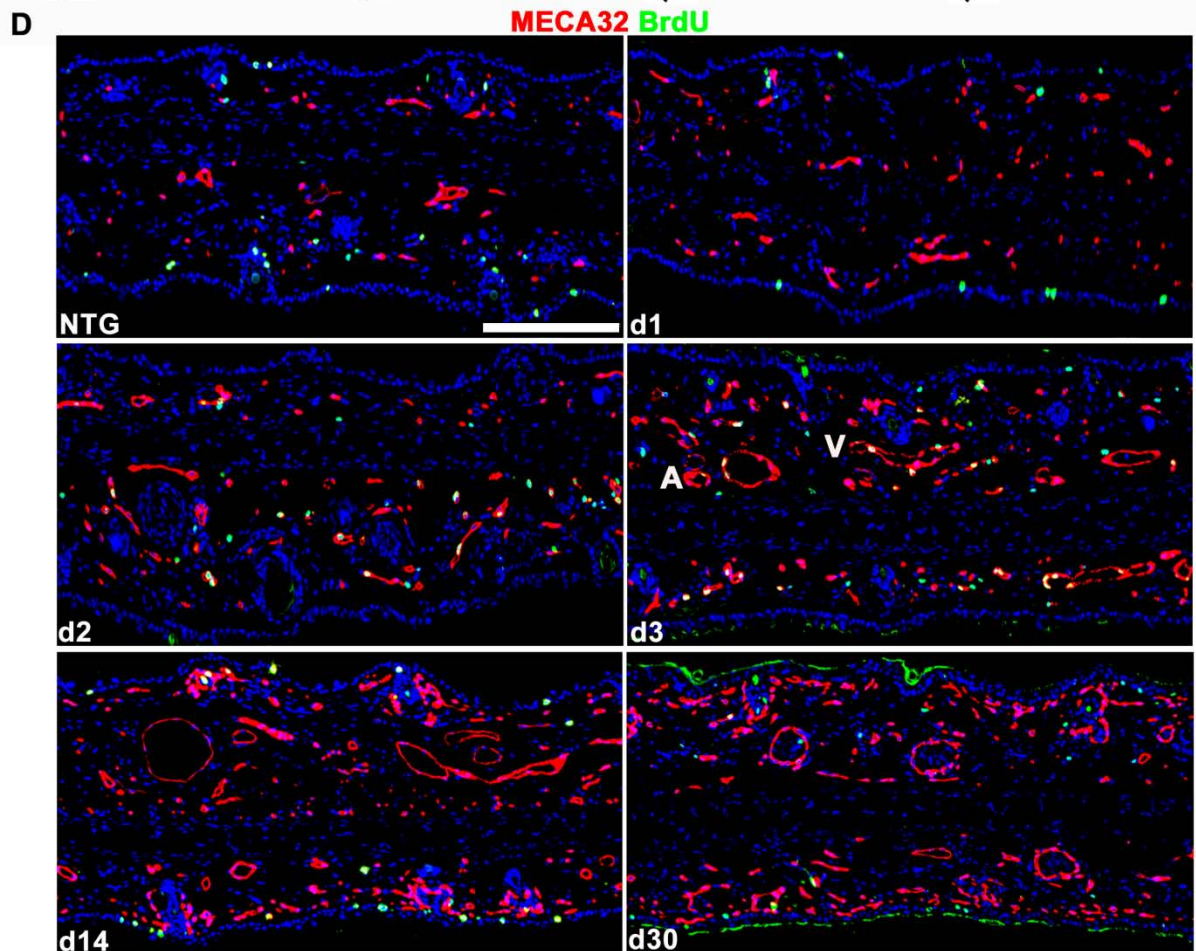
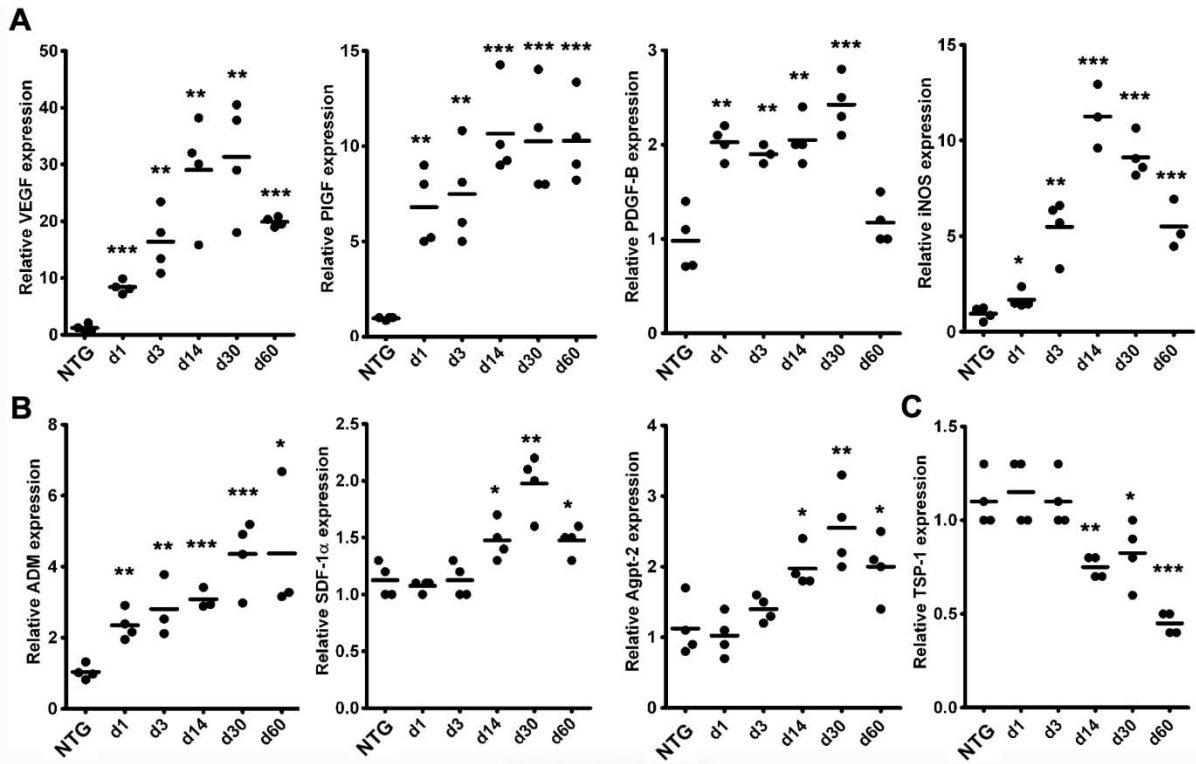


Figure S4. DOX induction of HIF-1 pro- and anti-angiogenic target genes, and endothelial/perivascular cell proliferation

(A–C) RT-PCR determination of differential patterns of HIF-1 target gene mRNA upregulation (A–B), or diminution (C). (D) Dual MECA32/BrdU immunofluorescence demonstrating activation of endothelial proliferation 36–48hr following DOX provision, peak proliferation on d3 and decrease to baseline by d30–60. Proliferation is detected in arteries and veins (representative vessels marked “A” and “V” in figure). TetON-HIF-1 data at each DOX day were compared with NTG, using unpaired Student’s t-test (**P<0.001, **p<0.01, * P<0.05). Bar: 200 μ m.

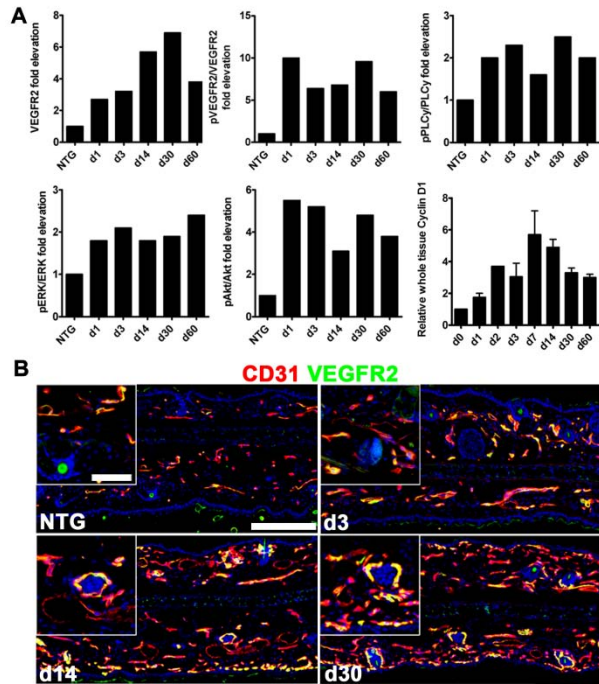


Figure S5. Epithelial HIF-1 activation results in persistent VEGF-VEGFR2 signaling pathway activation

(A) Quantification of Western blots detecting total VEGFR2, differential phosphorylation of VEGFR2^{Y1173}, PLCγ^{Y783}, ERK^{T202/204}, AKT^{S473}, and cyclin D1 induction and persistence.

Immunoblots were adjusted for sample loading based on β-tubulin densitometry, and then ratios of phospho- to total proteins were normalized to nontransgenic DOX or TetON-HIF-1 d0 ratios. Graphs are representative of 2–4 independent experiments. Tissue cyclin D1 data are mean ± SEM. (B) Dual CD31/VEGFR2 immunofluorescence shows progressive total VEGFR2 upregulation, with redistribution and persistent VEGFR2 expression in perifollicular endothelial cells. Bars: (B), 200 μm, inset 50 μm.

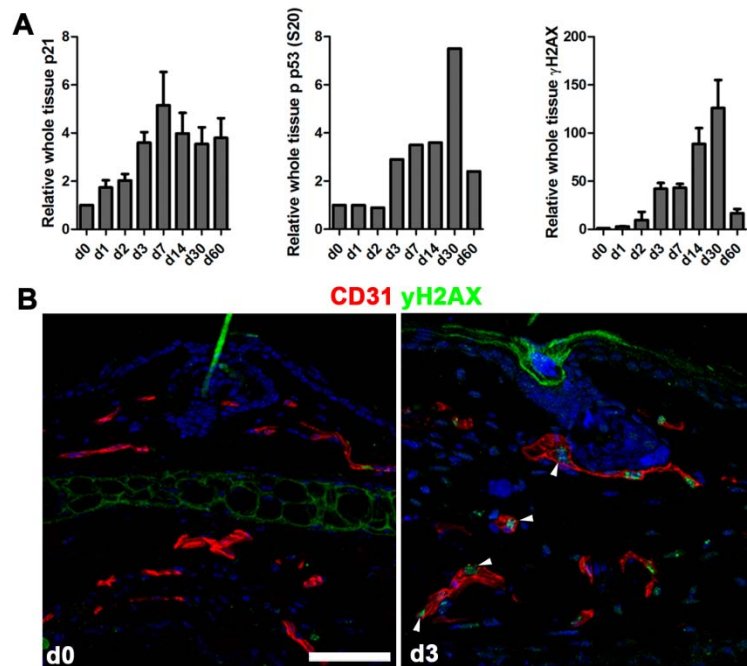


Figure S6. Identification and quantification of endothelial cell replication stress in response to HIF-1 induction

(A) Quantification of immunoblots presented in Figure 4. Graphs are representative of 2–3 independent experiments. Data are mean \pm SEM. (B) Representative confocal fluorescent images of γ H2AX localized to nuclear foci in d3 TetON-HIF-1 endothelial cells. Bar: 50 μ m.

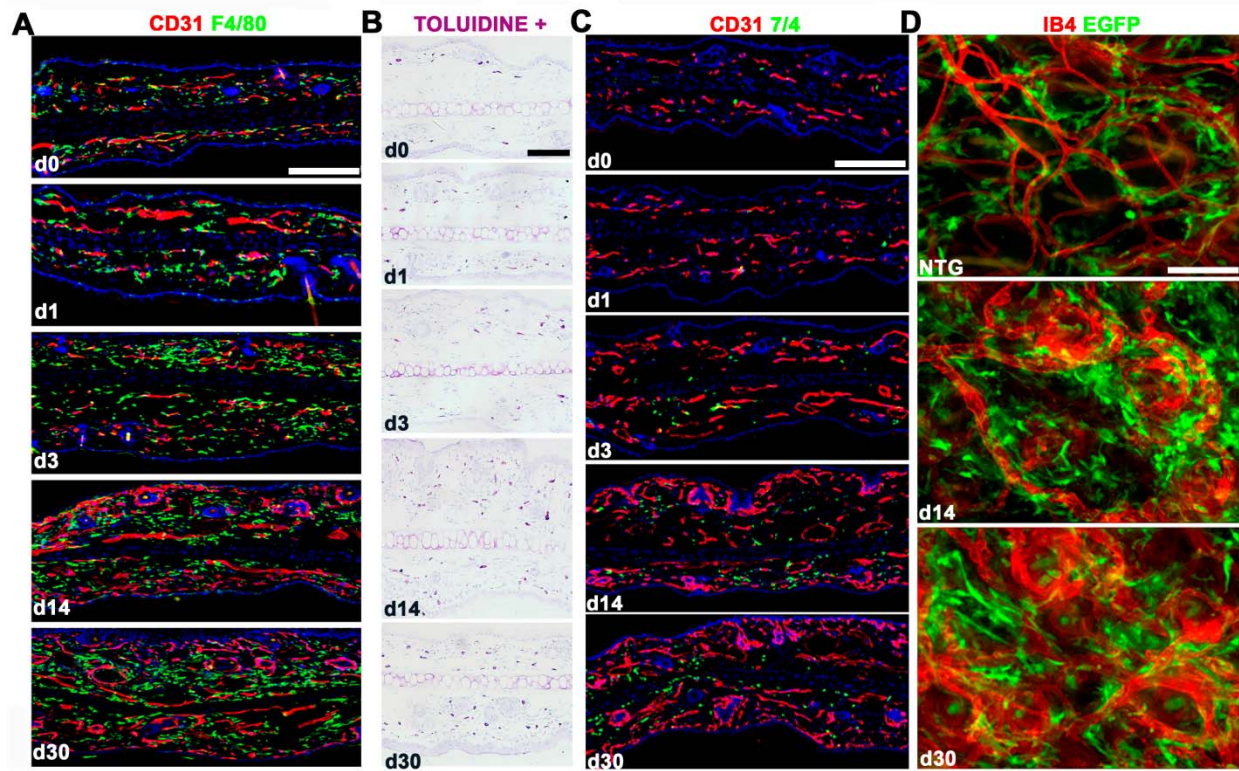


Figure S7. DOX induction leads to stromal macrophage, mast cell, neutrophil, and bone marrow-derived cell recruitment

(A) Dual CD31/F4/80 immunofluorescence demonstrating d0–14 macrophage recruitment and d14–28 retention in TetON-HIF-1 transgenic mice. (B–C) Mast cells [toluidine blue (+)] are also recruited and retained from d0–30 (B), though to a lesser extent than 7/4(+) neutrophils (C). (D) Differential perivascular GFP(+) bone marrow derived cell recruitment and retention. *In vivo* isolectin B4 (IB4) perfusion delineates the microvasculature. Bars: (A–C) 200 μ m; (D) 100 μ m.

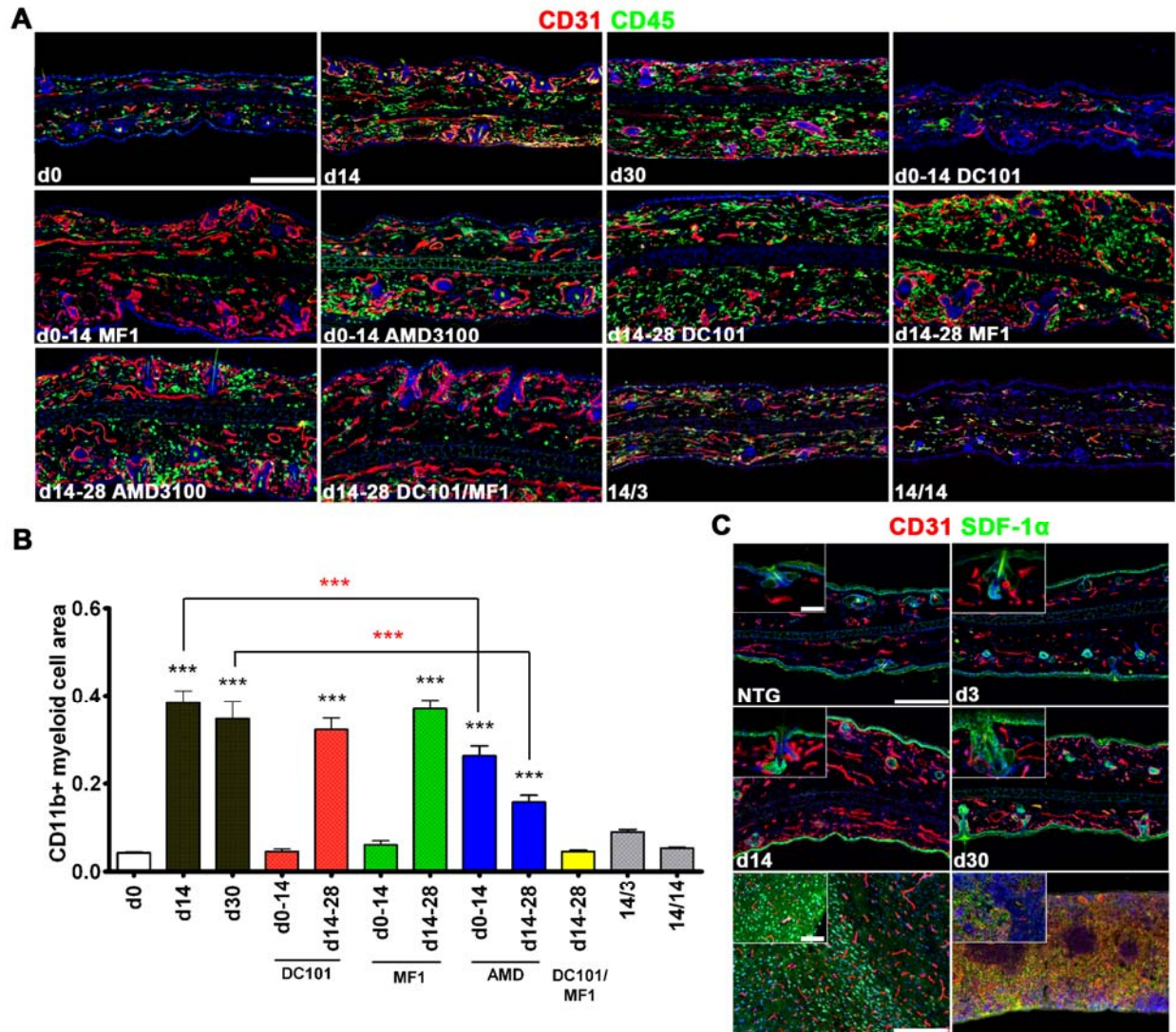


Figure S8. DOX induction leads to increased stromal CD45⁺/CD11⁺ myeloid cell recruitment and SDF-1 α expression

(A) Representative CD31/CD45 co-immunofluorescence demonstrating recruitment and stromal accumulation of CD45 myeloid cells during the TetON-HIF-1 DOX d0-14 neovascular development stage, with HIF-1-dependent retention of these cells from d14-28, similar to CD11b⁺ myeloid cell biology described in Figure 7A. Notably, CD11b⁺ myeloid cell recruitment and retention are differentially impaired by AMD3100. (B) Quantification of stromal area occupied by CD11b⁺ (n=3-4 mice per time point, see Figure 7A for representative immunofluorescent images). One-way ANOVA with Bonferroni's *post hoc* test showed that AMD3100 caused a significant decrease in CD11b⁺ cells during recruitment (31%) and retention (54%), compared to non-treated DTG d0 mice (three red asterisks). (C) Representative dual CD31/SDF-1 α immunofluorescence of ear cross sections showing incremental SDF-1 α expression from d3-14, plateauing at d30 in TetON-HIF-1 compared to NTG mice. Notably, SDF-1 α upregulation is predominantly restricted to basal keratinocytes, with rare endothelial cell

SDF-1 α co-immunofluorescence (top four panels and insets). Robust SDF-1 α expression in positive control tissues, brain (bottom left panel) and splenic cortex (bottom right panel). TetON-HIF-1 data at each DOX day were compared with TetON-HIF-1 d0 data, using One-way ANOVA with Bonferroni's *post hoc* test (***) $P < 0.05$). Bars: (A and C main panels), 200 μm . (C) 50 μm , upper four insets, 100 μm , lower two insets.

REFERENCES

1. Rasband, W.S., ImageJ, U. S. National Institutes of Health, Bethesda, Maryland, USA, <http://rsb.info.nih.gov/ij/>, 1997–2009.
2. Elson DA, Thurston G, Huang LE, et al. Induction of hypervascularity without leakage or inflammation in transgenic mice overexpressing hypoxia-inducible factor-1alpha. *Genes Dev.* 2001;15:2520–2532.
3. Du R, Lu KV, Petritsch C, et al. HIF1alpha induces the recruitment of bone marrow-derived vascular modulatory cells to regulate tumor angiogenesis and invasion. *Cancer Cell.* 2008;13:206–220.
4. Zhang HF, Maslov K, Stoica G, Wang LV. Functional photoacoustic microscopy for high-resolution and noninvasive in vivo imaging. *Nat Biotechnol.* 2006;24:848–851.
5. Hu S, Rao B, Maslov K, Wang LV. Label-free photoacoustic ophthalmic angiography. *Optics Letters.* 2010;35:1–3.
6. Wang L. Multiscale photoacoustic microscopy and computed tomography. *Nature Photonics.* 2009;3:9.
7. Yao J, Maslov K, Hu S, Wang LV. Evans blue dye-enhanced capillary-resolution photoacoustic microscopy in vivo. *J Biomed Opt.* 2009;14:054049.